# Microporous Carbon–Nitrogen Fibers from Keratin Fibers by Pyrolysis

**Erman Senoz, Richard P. Wool**

*Chemical Engineering Department, University of Delaware, Newark, Delaware 19716*

Received 19 October 2009; accepted 6 March 2010
DOI 10.1002/app.32397
Published online 7 June 2010 in Wiley InterScience (www.interscience.wiley.com).

**ABSTRACT:** A two-step pyrolysis method was developed for poultry keratin fibers to convert them into high temperature resistant and adsorbent fibers while retaining their original physical appearance and affine dimensions. Nearly all accessible pores in the microporous pyrolyzed chicken feather fibers (PCFF) have a diameter less than 1 nm and could be used in applications, such as adsorption, hydrogen storage, and separation of small gas molecules. An intermolecular crosslinking mechanism in the first step of pyrolysis at 215°C for 24 h provided an intact fibrous structure with no subsequent melting. The second step of the pyrolysis at 400–450°C for 1 h resulted in a microporous material with a narrower pore size distribution than commercial activated carbons. Surface and bulk characterization techniques including XPS, total carbon–nitrogen, and FTIR were utilized to examine property changes occurring during the two pyrolysis steps. A partially cyclic carbon–nitrogen framework (carbon/nitrogen ratio = 2.38) supported by double and triple bonds, and oxygen functionalities is the suggested structural model for the PCFF. © 2010 Wiley Periodicals, Inc. J Appl Polym Sci 118: 1752–1765, 2010

**Key words:** bio-based materials; keratin; chicken feather fibers; protein crosslinking; microporous; hydrogen storage

## INTRODUCTION

Over the ages, the adaptation of living organisms to harsh environmental conditions and inevitable natural selectivity produced biological materials with excellent properties such as spider silk[1] and avian feathers.[2] Chicken feathers have interesting properties, which we explore in this article. Although certain mechanical and chemical information about the chicken feathers is available,[2–5] their properties have not been investigated sufficiently to produce materials suited for micro or nano scale applications, such as material storage, separation, and electronics. On the other hand, a much higher number of studies[5–7] can be found on another keratin-based material, wool, simply because of its ease of processing and extensive utilization in textiles. In this regard, chicken feathers are disadvantaged by their dissimilar segment development. Figure 1(a) illustrates the typical subsegments of a chicken feather. To ameliorate the feathers' processability and focus on these subsegments, a recent technique[8] allows the separation of the thicker shaft composed of rachis and calamus from the thinner ramus (~ 6 μm diameter). In this article, the ramus section will be referred to as chicken feather fibers (CFF). The separation of these two physically and chemically dissimilar sections provided an opportunity to investigate them individually. For example, in the previous work by Hong and Wool[2] significant properties of chicken feather fibers were revealed, such as its low dielectric constant, low density, and fibers' compatibility with soy resin to obtain green composite materials. A scanning electron microscopy (SEM) image of a CFF is shown in Figure 1(b).

To better understand how feather fibers may be utilized, it is important to examine their most basic properties. Feather fibers are composed largely of keratin and a small amount of lipids.[7,9] The fibers' backbone is formed from α-helix keratin—the long and flexible feather fiber attributes mimic the α-helix aminoacid sequence. β-sheet structured keratin fills the spacing between the α-helix tubes. Hydrogen bondings between separate segments of the aminoacid chains provide high strength to the material. Hollowness at both nano and micro levels due to the crystalline segments and hollow cylindrical microstructure provide a lower density than pure water, ~ 0.8 g/cm$^3$.[2]

Cellulose and lignin based precursors are the most popular materials for the production of highly porous activated carbon materials. Activation methods by chemical and thermal treatment provide these

*Correspondence to:* R. P. Wool (wool@udel.edu).
Contract grant sponsor: USDA-SCREES.
Contract grant sponsor: National Research Initiative of the USDA Cooperative State Research, Education and Extension Service; contract grant number: 2005-35504-16137.

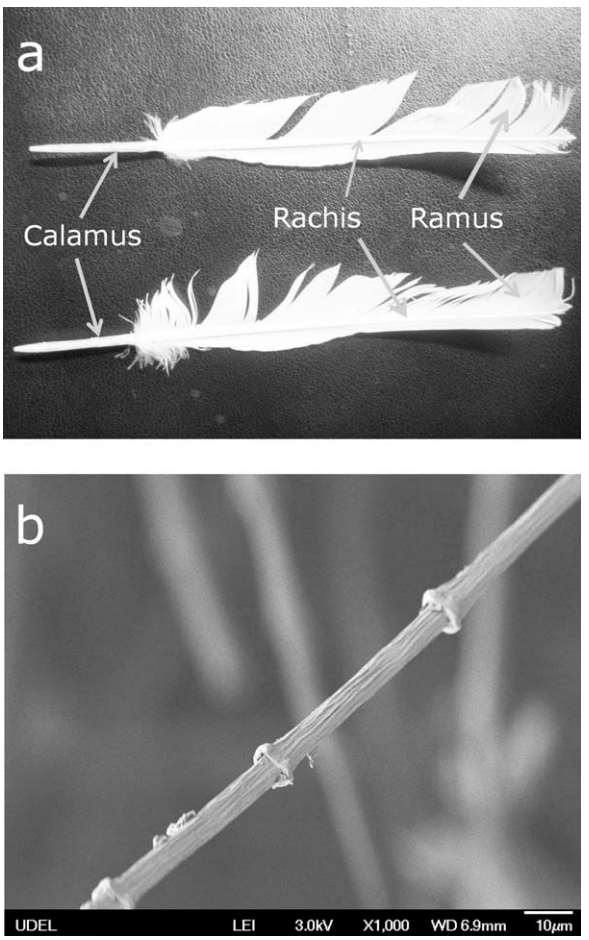


**Figure 1** The segments of chicken feathers (a), and the SEM image of an untreated chicken feather fiber (b).

materials with microporosity, high pore volume, and surface area typically in the range of 100–2000 $m^2/g$. These properties are crucial for the separation, purification, and storage of gases and liquids. Mezoporous materials are suitable for adsorption of larger molecules like hydrocarbons whereas microporous materials are helpful in smaller gas molecule applications, such as $H_2$, $CH_4$, CO, $CO_2$, $N_2$, and $O_2$ uptake.[10] Apart from thermal treatment of cellulosic precursors, various inorganic materials and organic polymers were investigated for microporous material production such as zeolites[11] and metal organic frameworks (MOFs).[12] Organic polymers of intrinsic microporocity (PIMs) with a phthalocyanine-metal base demonstrated high microporosity and surface area due to their rigid and contorted structure.[13] However, the literature does not demonstrate detailed studies on products from protein-based precursors containing nanoscale pores suitable for gas adsorption. The thermal treatment and the pyrolysis was studied on protein-based samples[14–17] only for the purpose of structural identification. The hollow nature of the CFF and their α-helix structure inspired us to use them as a precursor material for obtaining a uniform structured porous material. The use of CFF is desirable in this respect because they are protein-based materials originating from an abundant and essentially free renewable source. Due to the growing poultry industry, feather generation in the U.S. reached 4 billion pounds per year.[18] To note, most feathers are disposed of by burying or burning and the rest are converted to animal feed. Their utilization as an effective adsorbent material would actually alleviate a burden for the community.

Pyrolysis of linear polymers results in significant morphological changes including side-chain degradation or chain scission reactions. The side group reactions occur before the chain scission at relatively lower temperatures.[19] At elevated temperatures diverse reaction pathways, caused by the formation of free radicals,[19] occasionally provides increased surface area. Particularly for protein-based materials crosslinking mechanisms also play an important role in the determination of the final product. Instead of the carbon back bone, it is more suitable to focus on the carbon-nitrogen backbone.

In this study, the methods of developing carbon–nitrogen based fibers from CFF by controlled pyrolysis were investigated experimentally. The effects of maximum pyrolysis temperature levels and the isothermal heating below the crystalline melting point were studied. No chemical activation method was utilized. The possibility of obtaining an adsorbent material was particularly sought due to the hollow nature of CFF. The CFF were analyzed by differential scanning calorimetry (DSC) and thermal gravimetric analysis (TGA) to understand their general degradation behavior at high temperatures. Scanning electron microscopy (SEM) and $N_2$ adsorption techniques provided information on the porosity and physical properties. The fibers obtained from different points of the two-step pyrolysis method were characterized by X-ray photoelectron spectroscopy (XPS), total carbon–nitrogen atomic analysis and Fourier transform infrared (FTIR) spectroscopy techniques.

## EXPERIMENTAL

### Sample preparation

The Featherfiber Corporation (Nixa, MO) provided CFF that were already separated from the quill. The feather fiber separation method[8] is patented by the USDA. The density of the CFF was measured by a pycnometer and the displacement of water.

A thermolyne Type F6000 box furnace with a volume of 861 $in^3$ was used for pyrolysis. CFF were pyrolyzed with a constant 100 mL/min $N_2$ flow through the furnace. A constant $N_2$ flow was

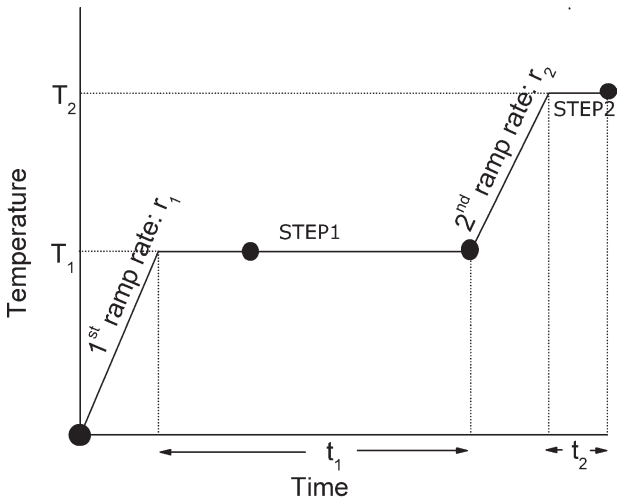


**Figure 2** A general temperature profile with respect to time in two-step pyrolysis. The highlighted points on the profile show the instances when the four samples were taken for elemental characterization.

provided for 3 h before the temperature ramps to minimize the oxygen concentration. The CFF were placed as a thin layer into flat bottom crucibles with a diameter of 6.25″. The weight fraction of the material at the end of the pyrolysis was greatly dependent on the initial CFF mass. The residue fraction variation was a consequence of the extremely low heat conductivity of the keratin-based feathers.[5] Large amounts of feather fibers making contact in a crucible have great potential to resist heat flow in the bulk. Therefore, in all cases in this study, 5 ± 1 g of precursor CFF was used to provide homogeneity and consistency. The weight fractions were calculated based on the consecutive three samples. The pyrolysis was achieved through two key steps as shown in Figure 2.

### The first step of pyrolysis at 215°C

The pyrolyzed CFF in Table I (including only the step1 in Fig. 2) were prepared to investigate the effect of an isothermal heat treatment at 215°C.

**TABLE I**
**PCFF Samples to Investigate the Effect of the Isothermal Segment at 215°C and Corresponding Residue Fractions**

| Sample | Temperature profile | Residue fraction |
|---|---|---|
| PCFF-1 | 3°C/min to 215°C and 2 h soak at 215°C | 0.767 ± 0.019 |
| PCFF-2 | 3°C/min to 215°C and 4 h soak at 215°C | 0.722 ± 0.012 |
| PCFF-3 | 3°C/min to 215°C and 10 h soak at 215°C | 0.638 ± 0.016 |
| PCFF-4 | 3°C/min to 215°C and 15 h soak at 215°C | 0.626 ± 0.011 |
| PCFF-5 | 3°C/min to 215°C and 24 h soak at 215°C | 0.601 ± 0.015 |

### The second step of pyrolysis

The purpose of this part of our study was to investigate the effect of higher temperatures (>220°C) on the CFF after the first step of the pyrolysis and to examine the possibility of obtaining a microporous material with high surface area. Figure 2 demonstrates the general method of preparation of different PCFF samples including the second step of pyrolysis. Table II lists corresponding parameters in the preparation of each sample, the residue fractions at the end and their final physical appearances. These methods were inspired from a previous study in our lab.[20]

Pyrolyzed chicken feather fiber (PCFF) samples were cooled down below 100°C in 3 h in $N_2$ atmosphere. They were washed with 100 mL of toluene and 300 mL of water, then dried overnight under a vacuum at 60°C to obtain the final product. Commercial activated carbons, Darco KB-G, and Darco G, were supplied by Sigma-Aldrich.

## Thermal analyses

Thermal analytical techniques were utilized to obtain degradation properties of the CFF. The untreated CFF were analyzed by a Mettler Toledo DSC 1 with an intracooler and a FRS5 sensor in a nitrogen atmosphere. Sample sizes ranged between 1.50 and

**TABLE II**
**The Pyrolysis Parameters with the Residue Fraction, Physical Appearance, and Absorbance Quality of the Final PCFF Products**

| Sample | $r_1$ (°C/min) | $T_1$ (°C) | $t_1$ (h) | $r_2$ (°C/min) | $T_2$ (°C) | $t_2$ (h) | Residue fraction | Physical appearance | Adsorption capacity |
|---|---|---|---|---|---|---|---|---|---|
| PCFF-6 | 3 | 215 | 24 | 3 | 400 | 1 | 0.176 ± 0.015 | Black, intact | Best |
| PCFF-7 | 3 | 220 | 24 | 2 | 450 | 1 | 0.101 ± 0.020 | Shiny black, not intact | Best |
| PCFF-8 | 3 | 220 | 32 | 2 | 450 | 1 | 0.063 ± 0.010 | Shiny black, not intact | Best |
| PCFF-9 | 3 | 400 | 1 | – | – | – | 0.209 ± 0.007 | Shiny black, not intact | Medium |
| PCFF-10 | 3 | 220 | 5 | 3 | 400 | 1 | 0.212 ± 0.018 | Shiny black, not intact | Best |
| PCFF-11 | 3 | 215 | 24 | 3 | 500 | 1 | 0.011 ± 0.002 | Black-gray, not intact | Low |
| PCFF-12 | 3 | 220 | 26 | 2 | 500 | 1 | 0.004 ± 0.001 | Black-gray, not intact | Medium |
| PCFF-13 | 3 | 220 | 24 | – | – | – | 0.617 ± 0.022 | Brown, intact | Low |

3.00 mg. The nitrogen flow was always set to 50 mL/min. In the evaluation of the melting point of untreated CFF from DSC curves, the most important characteristic temperatures are the beginning of the melting ($T_b$), the extrapolated onset of melting ($T_m$), and the peak temperature ($T_p$),[21] which were calculated by STAR$^e$ Software. DSC analysis was conducted on three individual CFF samples and the characteristic temperatures were determined from the average and the standard deviations. TGA was conducted by a Mettler Toledo TGA/DSC1 with a high temperature furnace that had a maximum temperature of 1600°C. The TGA resolution was 0.1 μg. Both DSC and TGA analyses were done at a 10°C/min heating rate.

### Nitrogen adsorption

The pore structures of the PCFF samples were analyzed using a Micromeritics ASAP 2010 with $N_2$ as the analysis gas. The specific surface areas (SSA) of the samples were reported by the Brauner-Emmett-Taylor (BET) method.[22] The pore size distributions (PSD) were calculated by the Horvath-Kawazoe (HK) method[23] for microporous samples. Micropore volumes were calculated by using the t-plot method.[24] All samples were degassed at least 10 h at 250°C before each analysis.

### Characterization

XPS spectra were taken using a PerkinElmer ESCA 5500 with Al Ka X-ray source to get information on the surface composition and the functionalities. The energy was 49.95 and 23.50 eV for survey and high resolution scans, respectively. The surface elemental compositions were determined from the empirically derived sensitivity factors of individual atoms.[25] All spectra were calibrated by taking 285.00 eV as C1s reference. The standard deviations of the calculated atomic fractions were less than 0.015.

The total carbon/nitrogen analysis was performed in triplicate using an Elementar Vario-Max CN Analyzer (Elementar Americas, Mt Laurel, NJ). The bulk carbon/nitrogen (C/N) ratios were converted to atomic ratios to compare with surface elemental concentrations. The rest of the samples were assumed to be composed of only oxygen and hydrogen after the determination of total carbon and nitrogen values. The average and the standard deviations were calculated based on the triplicated experimental results.

The CFF and PCFF samples were examined by a JSM-7400F SEM operating at 3 kV accelerating voltage. They were coated with gold using a Denton Vacuum Desk IV to increase the surface conductivity of the samples.

The infrared spectroscopy was performed on an ATI Mattson Genesis Series FTIR. The samples were mixed with KBr powder and compressed into pellets before the analysis. Each sample was scanned 64 times with a resolution of 4 $cm^{-1}$. The analysis was repeated at least three times by using different samples prepared by the same method. No significant spectra variation was observed.

## RESULTS AND DISCUSSION

### Density measurements

Immediately after submerging the untreated CFF under water in a pycnometer, their density was calculated even lower than the apparent density of CFF, 0.8 $cm^3/g^2$. Due to the hollow nature of the CFF, after 14 days of submersion they sank to the bottom and the density of the fibers was calculated to be 1.4 $g/cm^3$. It seems the hydrophobicity and the surface tension initially hindered the diffusion of water molecules deep in the pores. The former low density value was the density including the hollow volume, and the spaces between fibers due to the hydrophobicity of the surface. The latter is the skeletal density with the assumption of 100% filling of the hollow structure with water. The comparison of the chicken feather fiber apparent density and the skeletal density shows that 43% of the fiber volume contains hollow space open to the ambient environment. Under the assumption of a hollow cylindrical CFF fiber with a diameter of 6 μm, the fiber wall thickness was calculated at 2 μm.

### Thermal analyses

The data from DSC and TGA of CFF provided critical information on the structural changes leading to the pyrolysis discussed in the following sections. Figure 3 shows both DSC and TGA curves of untreated CFF. The DSC curve of CFF up to 500°C shows two major endotherm peaks (troughs) and some fluctuations above 260°C. The fluctuations are mostly from rapid degradation of the keratin. The two major troughs were also highlighted by Barone et al.[4] The first trough is a relatively broader at 114°C and is due to $H_2O$ evaporation. The broadness of the trough indicates the existence of a wide range of binding energies of water to the protein matrix. This phenomenon is supported by Feughelman[5] with a protein-water model utilizing hydrogen bonding. The mass decrease due to the distinct water evaporation is also clear in the TGA curve below 120°C. The second trough at 233°C in the DSC curve is much sharper than the water evaporation trough. This trough is irreversible and attributed to the crystalline melting of the alpha helix or

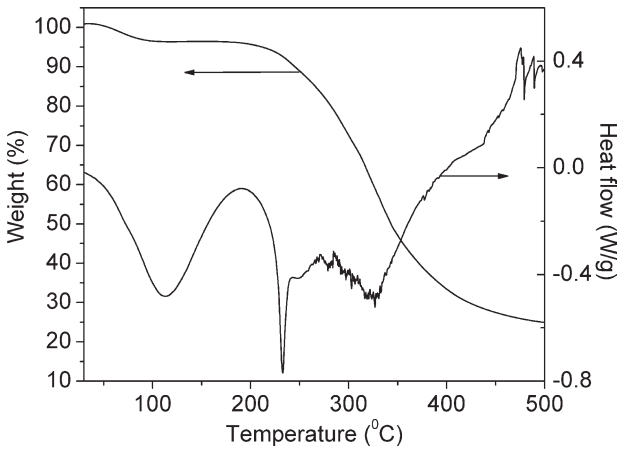


**Figure 3** TGA and DSC curves of untreated chicken feather fibers.

beta sheet protein.[4,6] The beginning of the melting ($T_b$), the extrapolated onset of melting ($T_m$), and the peak temperature ($T_p$) of the untreated CFF are 218.80 ± 1.71°C, 227.72 ± 0.69°C, and 232.70 ± 0.09°C, respectively. The variation for $T_p$ was much lower than $T_b$ and $T_m$. The variations in $T_m$ and $T_b$ can be explained by the slight dissimilarity and inhomogeneity in the semicrystalline structure of the samples. Furthermore, relatively high temperature gradients within the sample can also affect these errors.

In Figure 3, CFF undergoes a relatively rapid degradation in the range of 200 to 400°C. Above 400°C the fiber degradation slows down leaving a weight fraction of 0.28 at 450°C. Eventually, at 500°C the weight percent of the remaining material is as low as 25%. Therefore, a heat treatment above 400°C is required to achieve a high level of degradation through pyrolysis.

### The first step of pyrolysis at 215°C

The DSC results of PCFF-1–4 were compared with those of untreated CFF in Figure 4. It is important to note that 215°C the temperature at which PCFF samples were isothermally heat treated, is just below the crystalline melting starting temperature. The PCFF samples did not lose their water evaporation endotherm and still possess their water adsorption ability. However, the crystalline melting trough gets smaller and shifts up to a 10°C higher point as the isothermal heating period is increased. PCFF-3 and PCFF-4 do not show any crystalline melting. This change can be explained by a relatively slow crosslinking reaction in the crystalline alpha or beta structure. As crosslinking progresses, the different alpha helixes and crystalline beta planes bind to each other or to the amorphous protein matrix with their most active side functionalities forming a complex network. The carboxyl and amide side chain functionalities are very suitable for these crosslinking reactions. The recent piece of data from our ongoing research[26] by using a mass spectrometer coupled with a TGA demonstrated a high rate of $H_2O$ emission from the sample between 200 and 250°C. These results strengthened the probability of amide bond formation. Consequently, the crosslinked structure blocks the melting process and contributes to a more stable structural material for further heat treatment. Menefee and Yee[6] also demonstrated a rapid crosslinking mechanism at ~ 215°C in the polymer matrix of wool fibers, which also possess a similar keratin-based structure.

During pyrolysis the fibrous structure was retained except for a change in color. Heat treated fibers at 215°C turned from white to yellow and from yellow to brown. As the process continues the color continuously got darker. The PCFF-6 sample with a ramp to 400°C was homogeneously black. The diameters of the fibers shrank down to ~ 2 μm from their initial value of about 6 μm.

### The second step of pyrolysis

Inspired by the TGA analysis, a second pyrolysis step up to 400–500°C was inserted into the temperature profile to achieve a higher level of carbonization and increase the porosity by forming defects through degradation. The morphological changes were tracked to observe the effect of the first step of pyrolysis to the final fiber structure. The residue fractions at the end of the pyrolysis gave consistently lower values compared to the residual wt % obtained from TGA at the maximum temperature. It is important to note that TGA analysis is dependent more on temperature rather than time. Time gets

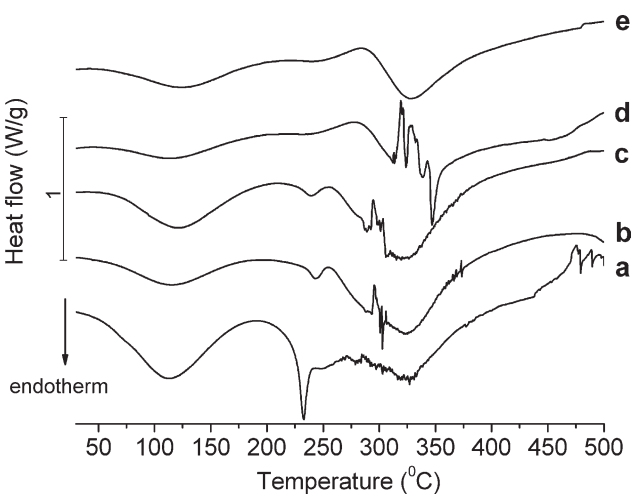


**Figure 4** Differential scanning calorimetry curves for untreated CFF (a), PCFF-1 (b), PCFF-2 (c), PCFF-3 (d), and PCFF-4 (e).

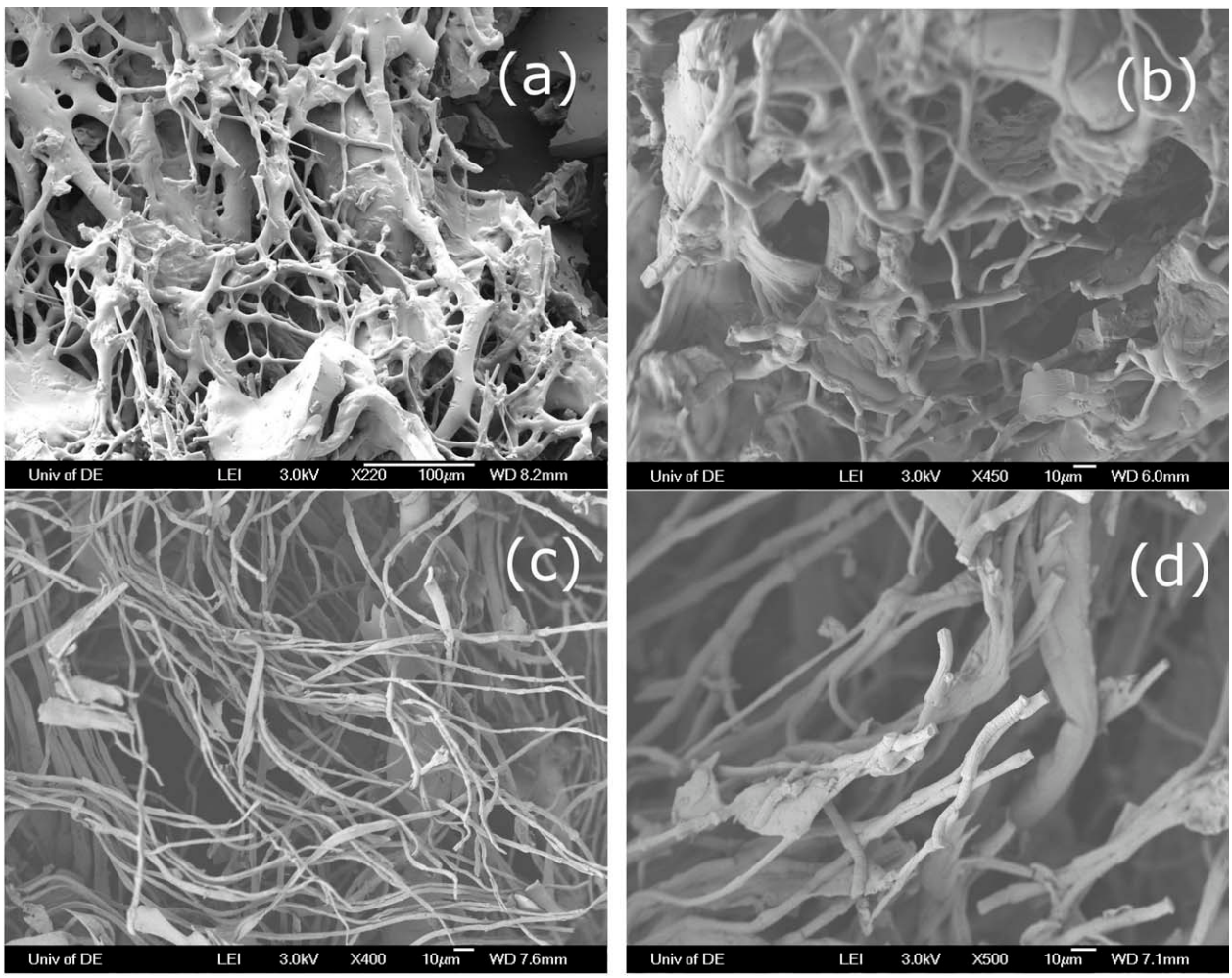


**Figure 5** The SEM images of PCFF-7 (a), PCFF-10 (b), PCFF-6 (c), and PCFF-13 (d).

incorporated into the pyrolysis analysis during the longer isothermal segments and slower ramp rates in the sample preparation. Therefore, pyrolysis is expected to give lower residue fractions than the TGA traces obtained at the same maximum temperature. On the other hand, small amount of oxygen trapped in the furnace during heat treatment may lead to a higher amount of degradation due to partial oxidation.

The physical appearances of the final products from the pyrolysis methods in Table II can be separated into two categories. PCFF-7, 8, 9 were all significantly different from untreated CFF and they fall into the first category: entirely black with some shining silver spots. [Fig. 5(a)] The fibers were clumped together and were highly breakable by a pestle and mortar. It was impossible to consider these samples as fibrous. PCFF-10 and PCFF-6 shown in Figure 5(b,c) were prepared to see the effect of less harsh pyrolysis conditions on the fibers. The PCFF-6 sample was considered to be in the second category in terms of its physical features. Although PCFF-6 had a much longer total heating time than PCFF-10, unlike PCFF-7, 8, and 10, the fibers were flexible and nearly unbreakable by using a pestle and mortar. No clumped fiber parts were observed. It was easy to separate the fibers from each other. This was a good indication that we successfully prevented the welding of fibers to each other by an intermediate melting. The first step of the heat treatment of PCFF-10 and PCFF-6 distinguishes these two methods. The comparison lead us to the fact that 220°C was sufficiently high to partially melt the fibers. The partially melted matrix tends to weld to each other causing the formation of fiber chunks, which is also clear on the SEM images. [Fig. 5(a,b)] An isothermal heat treatment at 215°C for the crosslinking mechanism that was explained in previous sections is recommended to avoid partial melting and to maintain the original feather fiber structure intact. Relatively harsher pyrolysis conditions were used in the preparation of PCFF-11 and PCFF-12 to test the thermal stability of the fibers. The quality of these samples was not at a desired level in terms of physical appearance. The samples were a fine gray powder. The method for PCFF-13 includes only the first step

**TABLE III**
**$N_2$ Adsorption Results**

| Sample | $S_{BET}$ ($m^2/g$) | $C_{BET}$ | $V_{mic}$ ($cm^3/g$) | Adsorption capacity |
|---|---|---|---|---|
| PCFF-6 | 436 ± 4 | 1003 | 0.178 | Best |
| PCFF-7 | 460 ± 2 | 6330 | 0.196 | |
| PCFF-8 | 419 ± 6 | 845 | 0.176 | |
| PCFF-10 | 376 ± 0 | 832 | 0.133 | |
| PCFF-9 | 189 ± 6 | 300 | 0.072 | Medum |
| PCFF-12 | 114 ± 0 | 822 | 0.041 | |
| PCFF-11 | 14 ± 0 | 68 | 0.002 | Low |
| PCFF-13 | <1 | 135 | <0.001 | |
| Darco KB-G | 1342 ± 6 | 205 | 0.416 | n/a |
| Darco G | 1124 ± 3 | 774 | 0.386 | |

$S_{BET}$, Specific surface area obtained by BET method[22] in the relative pressure range of 0.01–0.05; $C_{BET}$, BET constant; $V_{mic}$, Micropore volume calculated by t-plot method.

of the heat treatment. The original feather structure was retained except the color change from white to brown. However, the agglomeration of the fibers with a formation of fiber bundles was clear in Figure 5(d).

### Nitrogen adsorption analysis

The $N_2$ adsorption analyses on the two-step pyrolyzed CFF samples are presented in Table III. The final products were divided into three subgroups in terms of their adsorption capacity: Best, Good, and Low Capacity Adsorbents.

#### Best adsorbents

Higher surface areas and degree of microporosity were obtained from PCFF-6, 7, 8, and 10, which were heated up to 400 and 450°C in the second pyrolysis step. According to the IUPAC guidelines, the BET surface area calculations need to be presented within the relative pressure range of 0.05–0.3. It is also reported[27] that this range can be shifted to a slightly lower interval in cases of high adsorption energies. The SSAs by the BET method were determined in the recommended relative pressure range. However, the isotherms (PCFF-6, 7, 8, and 10) gave negative BET constants, which question the validity of the BET method for these samples. Therefore, as Kaneko and Ishii[28] proposed for microporous solids, a lower relative pressure range of 0.01–0.05 was used for linear fitting. Although, the BET constants were positive and meaningful at this range, it is still not suitable to derive conclusions from the specific surface area outputs. Due to the microporosity and existence of pore widths of not larger than a few $N_2$ molecule diameters, the BET model did not provide explicit SSA values. $S_{BET}$ values were reported in Table III for comparison purposes with other microporous materials in this article and in the literature.

IUPAC classifies adsorption isotherms according to the general trend of the curve. In this classification Type I isotherms show a rapid uptake at low relative pressures because of micropore filling and overlapping of interaction potentials of pore walls.[29] In higher relative pressures the gas uptake stays almost constant when all the micropores are filled. The $N_2$ adsorption isotherms of both PCFF-6 and PCFF-7 are Type I as demonstrated in Figure 6(a). Figure 6(b) gives the t-plots for PCFF-6 and PCFF-7. The statistical thickness of the adsorbed molecules is calculated by using the Harkins-Jura equation[30]:

$$t = \left( \frac{13.99}{0.034 - \log(\frac{p}{p_0})} \right)^{1/2} \quad (1)$$

The t-plot of the PCFF samples including the nonporous ones show the linear segment between 6.5–9 Å. Therefore a linear fit was consistently applied in the 6.5–9 Å interval. Extrapolation of the linear fit to the y-axis intercept gave the micropore contribution to the adsorbed $N_2$. It is important to note that the y-intercepts are 91.3 and 94.8% of the maximum $N_2$

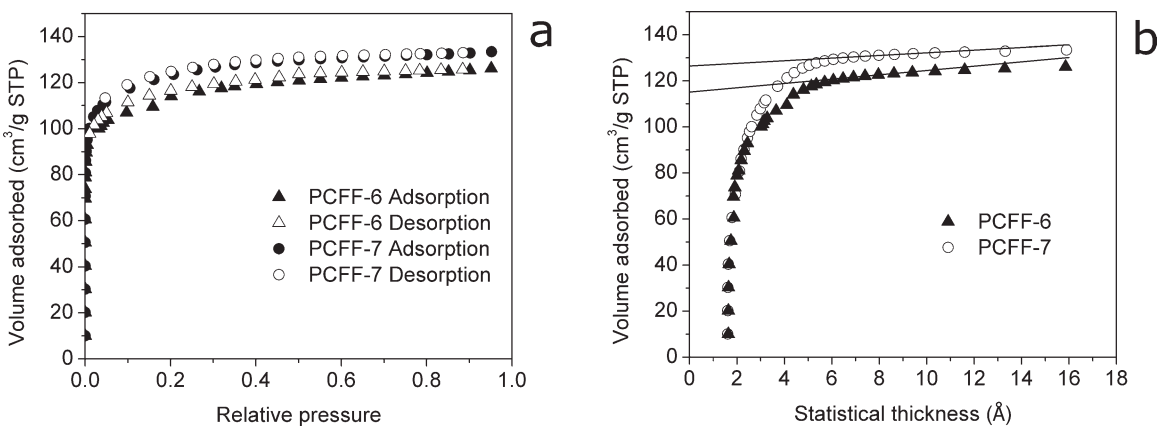


**Figure 6** $N_2$ adsorption and desorption isotherms (a) and t-plots (b) of PCFF-6 and PCFF-7.

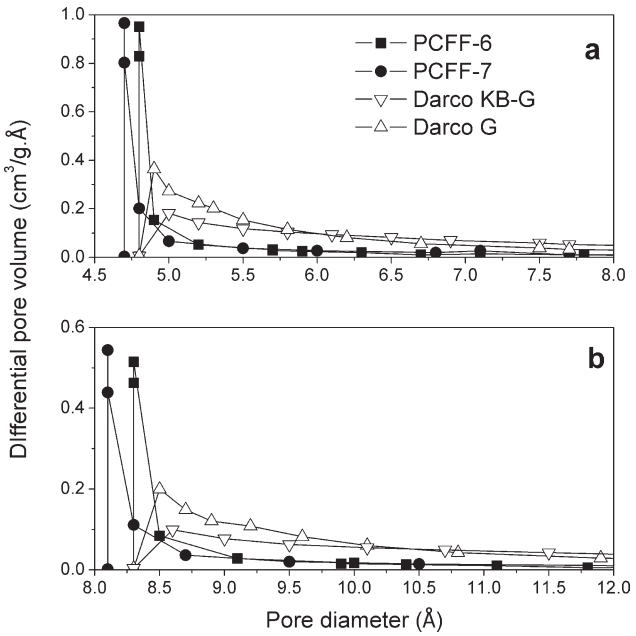


**Figure 7** Pore size distribution of PCFF-6, PCFF-7, and activated carbon samples (Darco KB-G and Darco G) by Horvath-Kawazoe method assuming slit[23] (a), cylindrical pore geometry[31] (b).

uptake for PCFF-6 and PCFF-7, respectively. The micropore volume of PCFF-7 reached up to 0.196 $cm^3/g$.

The microporosity of PCFF samples was also confirmed by the PSD of the samples. The PSD was calculated by the original HK method for slit shaped pores[23] and by a more recent modified version of the HK method for cylinder shaped pores.[31] In Figure 7 the PSD of PCFF are compared with the commercial activated carbon samples, Darco KB-G and Darco G, with high surface area and microporosity. The PSD of the micropores in PCFF-6 and PCFF-7 samples had a width range less than 0.5 Å in both cylindrical and slit pore assumptions. The two methods differed from each other by 3.5 Å in terms of the PSD curve maximum. According to our hypothesis there may be two reasons for these narrow range pores. The first one is that surface degradation provides access to micropores in the bulk. The second reason is that the structure alteration and rearrangement of the α-helix and beta sheet protein in such an orientation that will provide micropores. Both activated carbon samples showed a broader range of pore sizes compared to the PCFF samples. The existence of micropores within such a narrow pore size range suggests that the PCFF may have a selective adsorption or storage ability of certain small molecules. The preliminary $H_2$ adsorption results presented in GCE2009[26] showed that microporous PCFF could be a promising material for $H_2$ storage.

## Medium and low capacity adsorbents

The CFF that were heated to 400°C by single step, PCFF-9, have a micropore volume of 0.072 $cm^3/g$ with a significantly lower SSA than the best adsorbents prepared. The comparison of $N_2$ adsorption analysis of PCFF-6 and PCFF-9 revealed that inserting an isothermal segment below melting point at 215°C increased the microporosity of the fibers by a factor of more than 2. The high magnification SEM images of these two samples in Figure 8(b,c) also demonstrated important distinctions in the inner part of the twisted surface. PCFF-6 contained clearly visible cavities which could be connected to the micropores deep in the fiber.

Both PCFF-11 and PCFF-12 adsorption isotherms were Type II and lacked a high level of microporosity. PCFF-12 contained almost one fifth of the micropore volume of PCFF-7 whereas PCFF-11 is almost a nonporous material. This is an indication of micropore destruction when the temperature is raised up to 500°C. The nonporous PCFF-13 sample proved that a single step pyrolysis up to 220°C is not sufficient to open cavities and fractals on the surface. These results lead to the fact that the surface modifications and the degradation mechanism in the fibers between 220 and 450°C bring about a highly microporous structure. In general, all the samples prepared by two-step pyrolysis provided a significant level of porosity. Evaluating $N_2$ adsorption results

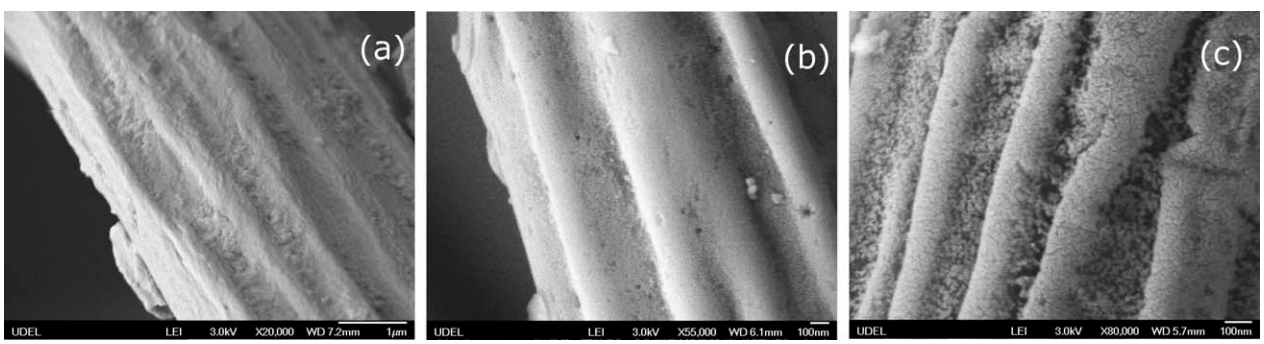


**Figure 8** High magnification SEM images of untreated CFF (a), PCFF-9 (b), and PCFF-6 (c).

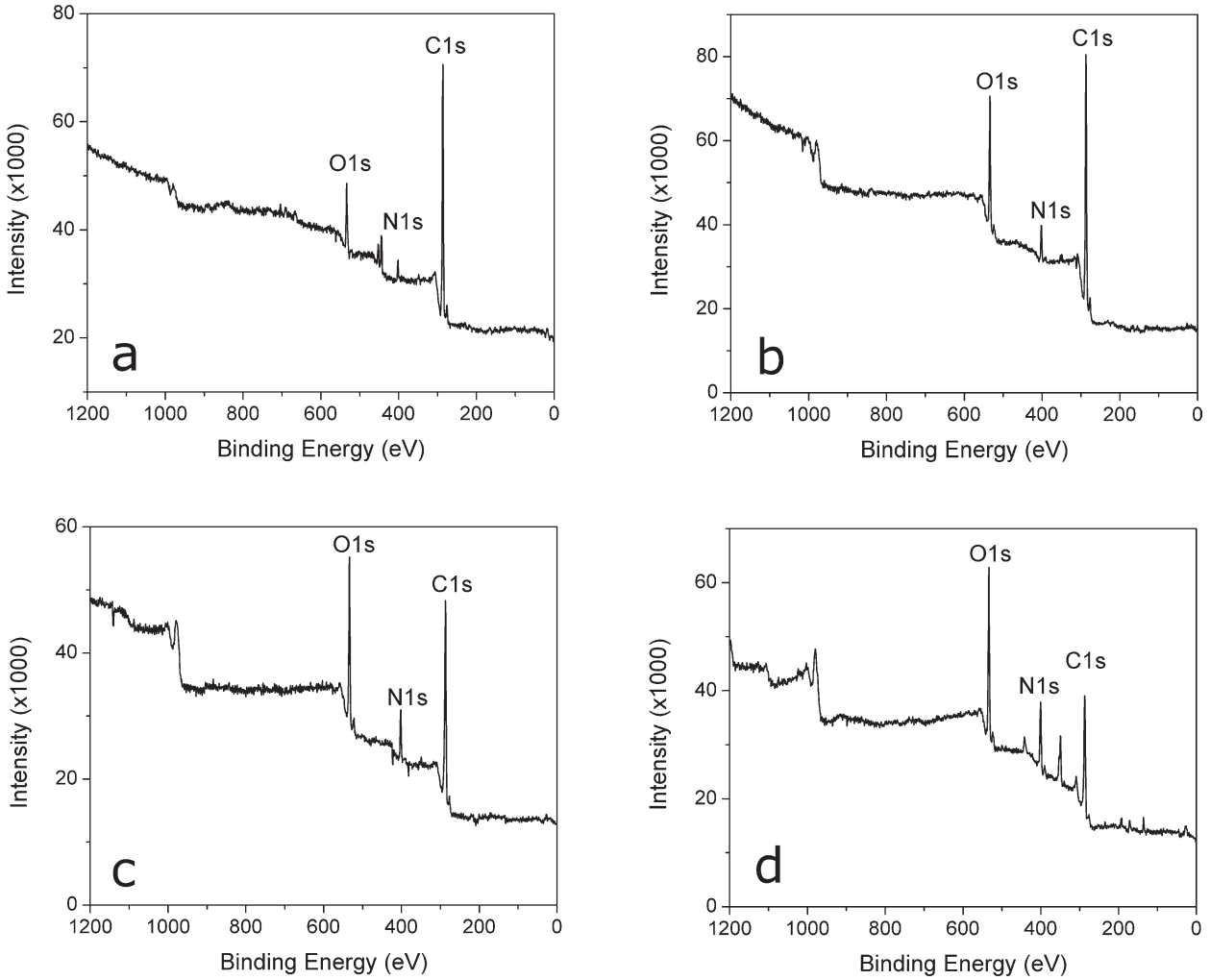


**Figure 9** XPS survey spectra of untreated CFF (a), PCFF-2 (b), PCFF-5 (c), and PCFF-6 (d).

from another point of view, the manipulation of the pyrolysis parameters to minimize the porosity of the fibers can also be useful for high performance fibers in composite applications. Consequently, in the future research moving towards obtaining good mechanical properties, the PCFF with two-step pyrolysis and a second step temperature below 400°C should be the suitable area of interest.

### Structural alteration determination during pyrolysis by surface and bulk characterization methods

#### XPS and total carbon/nitrogen analysis

Considering that pyrolyzed chicken feather fibers are a novel material, it is necessary to investigate their structure and formation. The structural characterization was accomplished by analyzing the surface (a few nanometers into the fiber) by XPS and the bulk (entire diameter 2–6 μm) by the total carbon–nitrogen analysis. The surface has a critical role because this section interacts with the ambient and may be connected to the micropores in the fiber bulk. Four samples (untreated CFF, PCFF-2, PCFF-5, and PCFF-6) were characterized by the surface and bulk characterization techniques. These are the samples prepared by the pyrolysis up to highlighted points in Figure 2, on the general pyrolysis profile.

XPS survey spectra of untreated CFF, PCFF-2, PCFF-5, and PCFF-6 were given in Figure 9. As expected C, O, and N form the basic elemental components of the samples. Sample PCFF-6 spectra also demonstrate the existence of small amounts of phosphate and sulfur. Sulfur can be found in the polymer matrix; however phosphate can be explained as an impurity. The untreated CFF and PCFF-6 spectra give an Indium peak at $\sim$ 443 eV. This peak is an effect of the Indium foil which the samples were pressed onto during the sample preparation. Table IV shows the surface and the bulk compositions of untreated and pyrolyzed CFF samples determined by XPS and the total carbon–nitrogen atomic analyzer, respectively. The comparison of the bulk and the surface makeup is limited to a degree due to the

**TABLE IV**
**The Elemental Surface (from XPS) and Bulk (from Total Carbon-Nitrogen Analysis) Concentrations of CFF and PCFF Samples**

| | Surface concentrations (at -H free) | | | | Bulk concentrations | | | |
|---|---|---|---|---|---|---|---|---|
| | C | N | O | C/N | TC (wt %) | TN (wt %) | T(O+H) (wt %) | C/N (at) |
| CFF | 0.874 | 0.040 | 0.086 | 21.85 | 0.532 ± 0.003 | 0.152 ± 0.006 | 0.316 ± 0.003 | 4.09 ± 0.20 |
| PCFF-2 | 0.804 | 0.061 | 0.135 | 13.18 | 0.551 ± 0.004 | 0.167 ± 0.002 | 0.282 ± 0.004 | 3.86 ± 0.05 |
| PCFF-5 | 0.682 | 0.111 | 0.207 | 6.14 | 0.553 ± 0.008 | 0.170 ± 0.006 | 0.277 ± 0.015 | 3.80 ± 0.09 |
| PCFF-6 | 0.519 | 0.185 | 0.296 | 2.81 | 0.569 ± 0.005 | 0.280 ± 0.019 | 0.151 ± 0.024 | 2.38 ± 0.14 |

basic principles of the techniques. Nevertheless, the techniques provide comparable carbon to nitrogen ratios (C/N) that are beneficial for the characterization.

The untreated CFF XPS survey spectrum has a large C1s peak, which contributes to 87% of the total elemental surface composition. More than five times higher C/N ratio on the surface compared to the bulk indicates that the surface has a different functionality. According to the model originated from the studies on wool fibers Negri et al.[7] suggested, the surface of keratin-based fibers contains a layer of fatty acids which also gives them the hydrophobicity and resistance to bacterial attacks. Randomly oriented carbon chains almost entirely cover the surface. This model clearly explains the excess carbon on the surface obtained by XPS. The C1s spectra in Figure 10(a) also support this model by showing a C=O functionalization. This peak is attributed to the acidic end of the fatty acid chains, which is connected to the polymer matrix mostly by covalent sulfur bonds. The sulfur peaks were below the noise

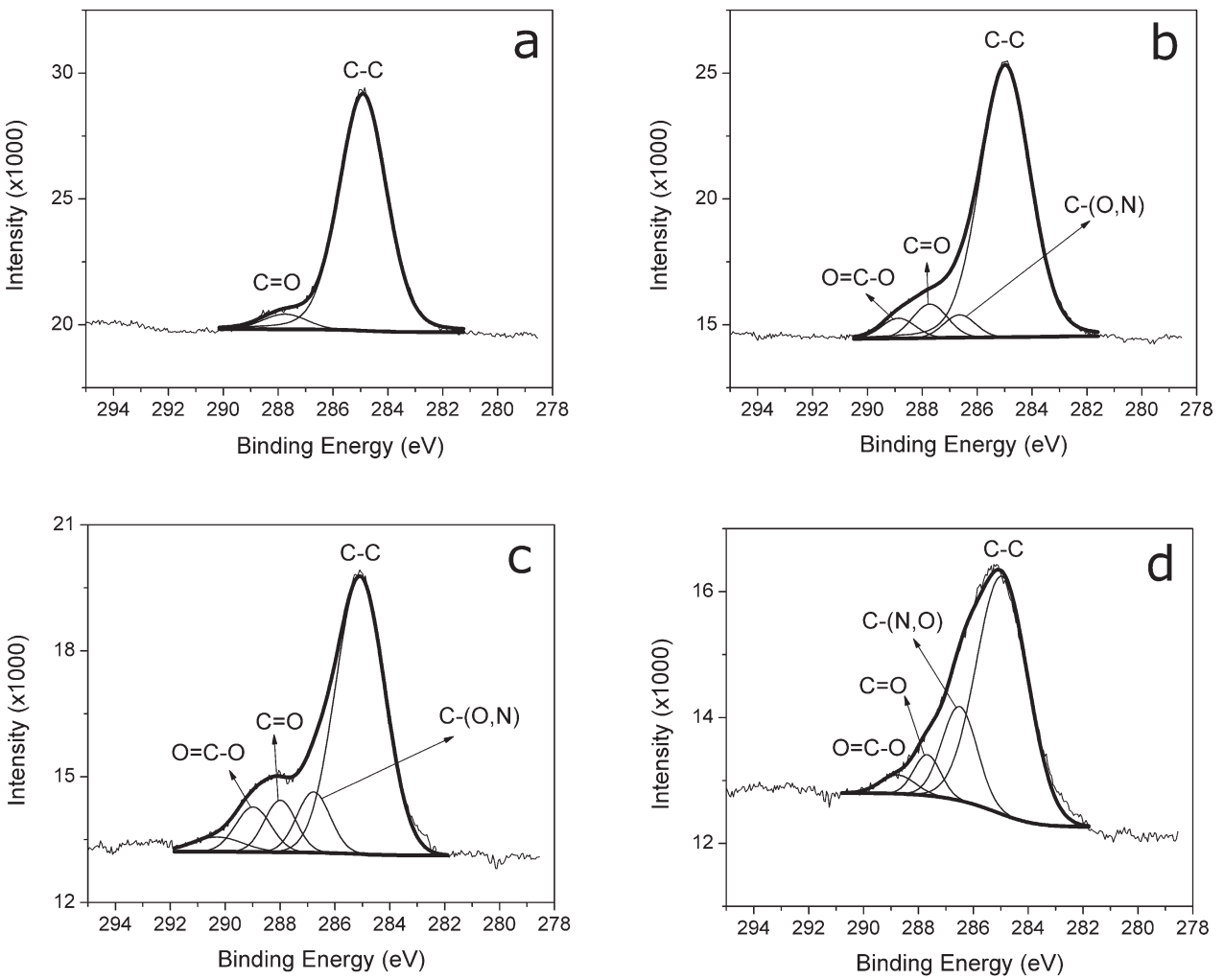


**Figure 10** Short range XPS C1s spectra of untreated CFF (a), PCFF-2 (b), PCFF-5 (c), and PCFF-6 (d).

level which could be due to screening by the monolayer fatty acid. The small amounts of N and O detected may stem from irregular distribution of the fatty acids and exposure of the protein matrix directly to the detector.

The studies in the literature vary on the amino acid distribution of the chicken feather keratin.[32,33] However, the contribution of the variation to the elemental composition of feather keratin was calculated to be insignificant. Both studies gave the C/N/O/H elemental weight fraction of 0.53/0.16/0.24/0.07. The untreated CFF total carbon–nitrogen results in Table IV were consistent with these numbers showing the accuracy of the analysis. This also suggests that chicken feather keratin bulk elemental compositions do not differ by large margins although they are composed of nearly up to 17 or 18 distinct amino acid residues.

The thermal treatment at 215°C for 4 and 24 h causes some significant changes on the fibers. On the surface, while the C/N ratio experiences significant drops from 21.85 to 13.18 and 6.14 respectively, the O/C ratio increases. This data strongly indicates partial decomposition of the fatty acid chains. The surface degradation eliminates the long carbon chains partially or shortens them, exposing more nitrogen and oxygen in the polymer matrix to the XPS detector. It is expected that the surface modifications and subsequent drop in surface carbon content are reflected in the bulk composition of the fibers as well. In the bulk, total oxygen plus hydrogen percentage and C/N ratio decreases. A mass balance calculation between untreated CFF and PCFF2 by taking bulk elemental compositions and the residue fractions (Table I) into account showed the percentage of elemental mass loss during the first 4 h of heat treatment at 215°C. While 25.2 and 20.4% of the total carbon and nitrogen were degraded respectively, the degradation of (H+O) is 35.8% of the initial (H+O). The higher degradation rate of H and O may be the consequence of an excess emission of gases such as $CO_2$ and $H_2O$. These excess pyrolysis gases might be the products of the partial oxidation and crosslinks of the side chains result from amide bond formation and esterification. The side chain degradation must be the dominant reaction path as hydrogen and oxygen are abundant in side groups compared to keratin backbone. The combination of the aforementioned factors results in a C/N ratio decrease from 4.09 to 3.80 in the keratin matrix.

Bulk elemental concentrations of PCFF heated at 215°C for 4 and 24 h (PCFF-2 and PCFF-5) showed slight variation. The calculated elemental degradation percentage of PCFF-5 compared to PCFF-2 was 16.6, 15.7, and 17.7% for C, N, and (O+H), respectively. The percentages do not show significant difference indicating that crosslinking reaction rates slow down. A rather random degradation mechanism takes place between 4th and 24th h of heat treatment instead of the existence of a dominant reaction. The surface fatty acid chain scission and breakage on the surface continue during this isothermal treatment, as can be derived from the C/N decrease on the surface.

Remarkably lower C/N ratio in PCFF-6 suggests considerable chemical modifications in both the bulk and surface structure. With a high level of degradation the C/N ratio in the bulk decreases from 3.80 to 2.38. It should be noted that the backbone of amino acid chains has the C/N ratio of 2/1. Therefore it is highly probable that the side chain groups have a higher affinity to detach from the structure between 215 and 400°C, which lowers the C/N ratio down to the 2/1 level. The surface C/N ratio is still higher than the bulk ratio. The rearrangement of the partially degraded surface lipids on the upper layer of the fibers can explain this difference. These rearrangements may also include some chemical reactions of the partially degraded fatty acids with the protein matrix. This is also confirmed by the high C-(C,H) peak in the C1s spectra in Figure 10(d). The surface contains a high amount of oxygen compared to the bulk. It is quite likely that the PCFF-6 sample is very vulnerable to oxidation due to various functionalities existing on the complex structured surface. Oxygen exposure from small amount of trapped air in the furnace during heat treatment may result in such a high amount of O concentration.

The C1s peak regions were analyzed by assigning five types of binding energy regions: C—(C,H) ($\sim$ 285.0 eV), C—(O,N) ($\sim$ 286.6 eV), O—C—O, C=O ($\sim$ 287.9 eV), O—C=O ($\sim$ 288.9 eV), and $\sim$ 290.3 for higher binding energy functionalities such as N—C—OOH. These peak energies are consistent with the XPS analysis of similar organic samples in the literature[34–36] within 0.1 eV. The outcomes of the C1s spectra for the samples heat treated at 215 and 400°C were consistent with the XPS survey spectra of the corresponding samples in terms of elemental compositions. (Fig. 10) In general, as the CFF were pyrolyzed at 215°C and further at 400°C, the C1s peak broadened roughly between 286 and 292 eV. The slow degradation of the fatty acid molecules on the surface and the exposure of the keratin polymer matrix can account for the broadening effect due to the more complex functionalities existing in the keratin matrix. Additional O=C—O and C—(O,N) peaks appear in PCFF-2 and PCFF-5 samples indicating detection of the polymer matrix. Moreover, O=C—O peak might be an indication of surface oxidation due to a small amount of oxygen similar to PCFF-6. The PCFF-5 C1s spectra show even higher O=C—O,

C—(O,N), and C=O functionalities due to the degradation of the surface fatty acid chains. A significant raise in the 286.6 eV peak is noticed in the PCFF-6 spectra, which mostly stems from the high concentration of nitrogen and C—N backbone. A small peak of O=C—O shows up as a result of unreacted acidic side chains and functionalities in the rearranged and possibly oxidized fatty acid structure.

The complexity of the CFF structure and overlapping of various N and O functionality peaks on XPS C1s spectra hinder the exact determination of the surface composition. In this analysis the effect of long range functionalities on the binding energies were neglected. The long range functionalities can shift certain binding energies even higher and the broad peak obtained at $\sim$ 290.3 eV in PCFF-5 C1s spectra is a nice example of this effect.

## Fourier transform infrared spectroscopy

The FTIR spectra were measured to confirm the structural changes within the fibers. Figure 11 shows the FTIR spectra of untreated CFF, PCFF-2, PCFF-5, and PCFF-6. The characteristic protein vibrations were reflected in the FTIR results as amide I–III. Untreated CFF possesses a broad amide I band (1655 $cm^{-1}$) caused by the C=O stretching in the amide group, a broad amide II band (1530 $cm^{-1}$) partially from N—H bending and C—N stretching vibrations on the protein backbone and a small amide III band (1270–1220 $cm^{-1}$) contributed largely from C—N stretching, N—H bending and weakly from C—C stretching and C=O in plane bending.[37,38] Amide I–III bands give critical information on the protein conformation and backbone structure. Particularly, the strength and the length of hydrogen bonds can be qualitatively determined from the location of the FTIR bands and significant contributions can be made related to the secondary structure of the protein in question. For instance obtaining an amide I frequency of 1648–1660 $cm^{-1}$ is an indication of abundance of $\alpha$-helix conformation in the keratin matrix.[38] The amide III band is less effective in determining the protein structure due to overlapping side chain vibrations.[38] Furthermore, the broad band in the range of 3600 and 3100 $cm^{-1}$ and the band at 3075 $cm^{-1}$ result from the characteristic amide vibrations of N—H (amide A and B) and O-H in the side chains.

The signal intensity difference between samples hinders the direct comparison between samples. However, comparative analysis between the bands within the same sample can give us clues on the structural changes. PCFF-2 (heat treated at 215°C for 4 h) and PCFF-5 (heat treated at 215°C for 24 h) showed almost all the protein FTIR amide bands with no wave number shifts which is an indication

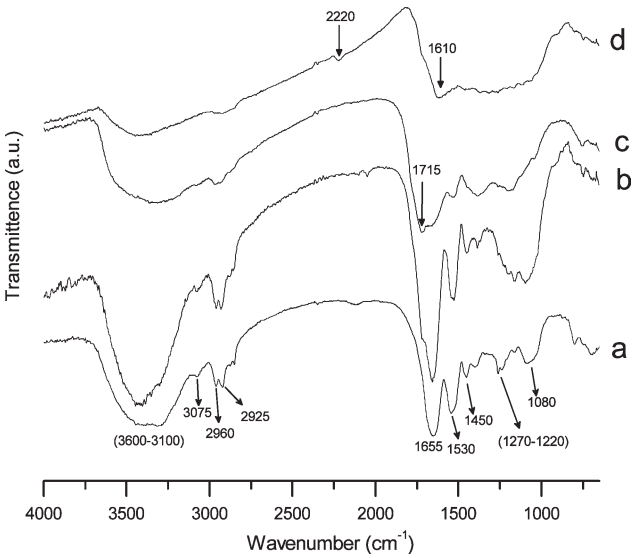


**Figure 11** FTIR spectra of untreated CFF (a), PCFF-2 (b), PCFF-5 (c), and PCFF-6 (d).

of intact protein structure. However, it was noticed that the amide II peak height decreased compared to amide I peak height as CFF was heat treated at 215°C. Additionally, the amide III band shrank. These suggested that either the N—H bond was broken or the C—N bond on the backbone was cleaved. If the latter is true then it is possible to speculate that the intermolecular crosslinking which was formed during heat treatment provided enough support for the fibers to retain their fibrous structure.

The untreated CFF spectra also demonstrate bands contributed from the side chain groups. A band between 3000–2840 $cm^{-1}$ including two transmittance troughs indicates side hydrocarbon chains. The asymmetric and symmetric C—H stretching ($CH_3$) reflects the spectra at 2960 and 2925 $cm^{-1}$, respectively.[39] Edwards et al.[39] demonstrate strong $CH_2$ scissoring bands at 1448 $cm^{-1}$ in various keratin materials. Untreated CFF sample shows this band at 1450 $cm^{-1}$. In heat treated CFF samples, PCFF-2 and PCFF-5, the heights of these bands also drop comparatively due to the fact that the previously mentioned dominant side chain scission cleaved the side chains leaving shorter side groups at medium level temperatures. The band at 1200–1000 $cm^{-1}$ is assigned to various skeletal C—C vibrations.[39,40] Untreated CFF possesses a broad band between 1120 and 1000 $cm^{-1}$. When CFF were heat treated at 215°C, this band got broader and extended up to 1200 $cm^{-1}$. It is expected to see a change in C—C bond vibration due to the slight modification of the backbone as a consequence of the aforementioned amide II and III band shrinkage. 1200–1000 $cm^{-1}$ region also overlaps with the C—O bond making it impossible to reach clear conclusions. On the other hand, a C=O vibration shoulder at 1715 $cm^{-1}$ from

carboxylic acids[40] appeared in the PCFF-2 and PCFF-5 spectra. This result is a consequence of a partial oxidation over time by transformation of some carbons to carboxylic acids and is parallel to the results obtained from XPS analysis.

The second step of pyrolysis altered the FTIR spectra noticeably as expected. (Fig. 11, PCFF-6) As demonstrated in total carbon–nitrogen analysis and XPS, the fibers lose the majority of their oxygen functionalities as a consequence of the degradation of oxygen groups (O—H, C=O, and COOH). With a high level of thermal degradation on the thermally crosslinked keratin the FTIR spectra of PCFF-6 showed a band at 1610 $cm^{-1}$ above which there are no significant C=O peaks. The region below 1625 $cm^{-1}$ is open to different interpretations because of the broadness of the peaks and the possibility of having different structures within the same band. However, the desaturation of the carbon and nitrogen seems inevitable when previous analyses in this article were also taken into consideration. Clearly, while weaker bonds were cleaved, stronger bonds will remain making the fiber more stable to high temperatures. The formation of double and triple bonds may result in bands between 1630 and 1575 $cm^{-1}$ (N=N strech)[40] and between 2260 and 2200 $cm^{-1}$ (nitrile group R—C=N stretch).[40] This is also consistent with the shrinkage of the C—H stretching vibrations in 3000–2840 $cm^{-1}$ showing desaturation of carbons and dehydrogenation. Furthermore, the skeletal carbon vibrations in the aromatic compounds can result in the bands at 1600 and 1580 $cm^{-1}$.[40] Finally, it is worth noting that a band at 1610 $cm^{-1}$ may well be a low amide I vibration. In cases of strong hydrogen bonding mostly due to the denaturation and degradation of the protein, C=O stretching vibrations may lower down to the 1628–1610 level.[38]

### Interpretation of the pyrolysis mechanism from bond energies

The basis of pyrolysis modifications and degradation on materials lie under the bond energies of the precursor. In principle relatively weaker bonds break during degradation and stronger bonds form remaining higher bond energies both in the gas products and degraded precursor. The emission of $CO_2$ and $H_2O$ is highly expected because the bonds forming these molecules are quite strong. (C=O: 192.1 kcal/mol, O—H: 111.8 kcal/mol).[41] In the CFF bulk the weakest bonds will break first. The degradation will be accompanied by formation of stronger bonds in PCFF. In this respect amino acid residues containing amine or sulfur side groups (Arginine, Lysine, Cysteine) are more vulnerable to degradation. N—C bonds on the side chains have energies in the range of 70–73 kcal/mol.[41] However, a faster crosslinking reaction may lead to the consumption of amine groups by formation of amide bonds with carboxylic acid chain ends. Amide bonds can exhibit higher bond energies reaching up to 100.1 kcal/mol.[41] The degradation is followed by Serine and Threonine side groups containing C—OH bond, which has 80–81 kcal/mol[41] bond energy and saturated side carbon chains (C—C: 84–85 kcal/mol).[41] The indications of the above degradation mechanisms (side group degradations) during isothermal heat treatment at 215°C were obtained from FTIR and total carbon–nitrogen analyses.

In the protein backbone, the weakest bond is the HN—$C_\alpha$ bond. C—$C_\alpha$ and amide bond seem stronger due to the neighboring C=O group.[41] Therefore the cleavage of the HN—$C_\alpha$ bond is more probable. However, a dehydrogenation reaction between nitrogen and carbon can also form a stronger bond keeping the backbone intact. Although a modification related to the amine bands on the backbone was detected from FTIR analysis, exact identification is not possible at this point.

The results of the review of the bond energies and the structural analysis of the PCFF heated up to the second step of the pyrolysis suggested that modification bring about a more temperature stable structure mostly made of carbon and nitrogen elements.

## CONCLUSIONS

A two-step pyrolysis method was developed to form micropores in the chicken feather fibers. The pyrolyzed chicken feather fibers prepared by a maximum temperature of 400–450°C had a narrower pore size distribution than commercial activated carbons. The PCFF's microporosity with a micropore volume of 0.196 $cm^3/g$ STP and a pore width of less than 1 nm rendered them exceptionally promising for future adsorption studies. The pyrolysis method consisted of two steps:

1. The first step involved the crosslinking of the protein chains similar to the transition process of a hard-boiled egg and stabilizes them physically. The bulk characterization techniques provided evidences of side-chain degradation accompanied by a modification of the protein backbone caused by the N—H and HN—$C_\alpha$ bonds.
2. The second step chemically modified the crosslinked keratin and the final product was a carbon–nitrogen fiber with oxygen functionalities supported by aromatic groups and double and triple bonds. The geometry of the crystals in the initial keratin fibers and their α-helix confirmation could account for the narrow pore size

distribution. The chemically bound fatty acid chains on CFF degraded during both steps of the pyrolysis.

Further studies on the selective gas adsorption or hydrogen storage capabilities of PCFF will be completed in the future. The high temperature stability of PCFF provided them an exceptional advantage over untreated CFF in finding an application.

We acknowledge Professor Raul Lobo for the technical advice and the experimental support especially in $N_2$ adsorption analysis and pyrolysis. We also thank Dr. Sergey Rykov for his help in XPS experiments and Featherfiber Corporation (Nixa, MO) for supplying feather fibers.

## References

1. Winkler, S.; Kaplan, D. L. Rev Mol Biotechnol 2000, 74, 85.
2. Hong, C. K.; Wool, R. P. J Appl Polym Sci 2005, 95, 1524.
3. Barone, J. R.; Schmidt, W. F. Compos Sci Technol 2005, 65, 173.
4. Barone, J. R.; Schmidt, W. F.; Liebner, C. F. E. J Appl Polym Sci 2005, 97, 1644.
5. Feughelman, M. Mechanical Properties and Structure of Alpha-Keratin Fibers: Wool, Human Hair and Related Fibers; University of South Wales Press: Sydney, 1997.
6. Menefee, E.; Yee, G. Text Res J 1965, 35, 801.
7. Negri, A. P.; Cornell, H. J.; Rivett, D. E. Text Res J 1993, 63, 109.
8. Gassner, G.; Schmidt, W.; Line, M. J.; Thomas, C.; Waters, R. M. U.S. Pat. 5,705,030 (1998).
9. Stettenheim, P. R. Am Zool 2000, 40, 461.
10. Yang, R. T. Adsorbents: Fundementals and Applications; John Wiley & Sons, Inc.: New Jersey, 2003.
11. Davis, M. E.; Lobo, R. F. Chem Mater 1992, 4, 756.
12. Rowsell, J. L. C.; Yaghi, O. M. Angew Chem Int Ed 2005, 44, 4670.
13. Budd, P. M.; Ghanem, B. S.; Makhseed, S.; McKeown, N. B.; Msayib, K. J.; Tattershall, C. E. Chem Commun 2004, 230.
14. Meuzelaar, H. L. C.; Haverkamp, J.; Hileman, F. D. Pyrolysis Mass Spectrometry of Recent and Fossil Biomaterials: Compendium and Atlas; Elsevier Scientific Pub. Co.: Amsterdam; New York, 1982.
15. Johnson, W. R.; Nedlock, J. W.; Hale, R. W. Tob Sci 1973, 17, 89.
16. Winter, L. N.; Albro, P. W. J Gas Chromatogr 1964, 2, 1.
17. Merritt, C.; Robertso, Dh. J Gas Chromatogr 1967, 5, 96.
18. Dossey, L. Explore J Sci Healing 2005, 1, 155.
19. Moldoveanu, S. C. Analytical Pyrolysis of Natural Organic Polymers; Elsevier: Amsterdam, 1998; Vol. 20, p 9.
20. McChalicher, C. W. J. Thesis, University of Delaware, Newark, DE, 2003.
21. Wunderlich, B. Thermal analysis; Academic Press: Boston, 1990; p 339.
22. Brunauer, S.; Emmett, P. H.; Teller, E. J Am Chem Soc 1938, 60, 309.
23. Horvath, G.; Kawazoe, K. J Chem Eng Jpn 1983, 16, 470.
24. Lippens, B. C.; Deboer, J. H. J Catal 1965, 4, 319.
25. Briggs, D.; Seah, M. P. Practical Surface Analysis: By Auger and X-ray Photo-Electron Spectroscopy; Wiley: Chichester; New York, 1983.
26. Senoz, E.; Wool, R. P. Presented at 13th Annual Green Chemistry and Engineering Conference; College Park, MD, 2009.
27. Sing, K. S. W.; Everett, D. H.; Haul, R. A. W.; Moscou, L.; Pierotti, R. A.; Rouquerol, J.; Siemieniewska, T. Pure Appl Chem 1985, 57, 603.
28. Kaneko, K.; Ishii, C. Colloids Surf 1992, 67, 203.
29. Gregg, S. J.; Sing, K. S. W. Adsorption, Surface area, and Porosity; Academic Press: London; New York, 1982; p 207.
30. Harkins, W. D.; Jura, G. J Chem Phys 1943, 11, 431.
31. Saito, A.; Foley, H. C. AIChE J 1991, 37, 429.
32. Szabo, I.; Benedek, A.; Szabo, I. M.; Barabas, G. World J Microbiol Biotechnol 2000, 16, 253.
33. Schmidt, W. F. Presented at Poultry Waste Management Conference; Springdale, AR, 1998.
34. Sabbatini, L.; Zambonin, P. G. J Electron Spectrosc Relat Phenom 1996, 81, 285.
35. Kingshott, P.; Thissen, H.; Griesser, H. J. Biomaterials 2002, 23, 2043.
36. Mitchell, R.; Carr, C. M.; Parfitt, M.; Vickerman, J. C.; Jones, C. Cellulose 2005, 12, 629.
37. Bandekar, J. Biochim Biophys Acta 1992, 1120, 123.
38. Jackson, M.; Mantsch, H. H. Crit Rev Biochem Mol Biol 1995, 30, 95.
39. Edwards, H. G. M.; Hunt, D. E.; Sibley, M. G. Spectrochim Acta Part A 1998, 54, 745.
40. Yadav, L. D. S. Organic Spectroscopy; Anamaya Publishers: New Delhi, India, 2005; p 67.
41. Sanderson, R. T. Chemical Bonds and Bond Energy; Academic Press: New York, 1971; p 142.